INTERNATIONAL JOURNAL FOR NUMERICAL METHODS IN FLUIDS
Int. J. Numer. Meth. Fluids 2000; **34**: 609–626

Motion of deformable drops in pipes and channels using Navier–Stokes equations

Ch. Kaliakatsos and S. Tsangaris*,[1]

Laboratory of Aerodynamics, National Technical University of Athens, Zografou, Athens, Greece

SUMMARY

The motion of deformable drops in pipes and channels is studied using a level set approach in order to capture the interface of two fluids. The interface is described as the zero level set of a smooth function, which is defined to be the signed normal distance from the interface. In order to solve the Navier–Stokes equations, a second-order projection method is used. The dimensionless parameters of the problem are the relative size of the drop to the size of the pipe or channel cross-section, the ratio of the drop viscosity to the viscosity of the suspending fluid and the relative magnitude of viscous forces to the surface tension forces. The shape of the drop, the velocity field and the additional pressure loss due to the presence of the drop, varying systematically with the above-mentioned dimensionless parameters, are computed. Copyright © 2000 John Wiley & Sons, Ltd.

KEY WORDS: deformable drop; level set approach; drop motion

1. INTRODUCTION

The motion of deformable drops in two-dimensional channels or in circular tubes is of interest in a variety of industrial, technical and biological applications. Much of the earliest interest in this subject was motivated by the suggested analogy between the drop motion and the motion of blood cells in capillary tubes.

This analogy was also the motive for us to perform this study. Actually, various models were used to simulate the single file flow of red blood cells in microcirculation. Poulou [1] modelled the red blood cells as rigid particles and studied the partitioning of these particles at divergent tubes. Queguiner and Barthes-Biesel [2] used capsules for modelling of red blood cells and studied the axisymmetric motion of capsules through cylindrical channels.

These flow systems also arise in many polymer processing operations, as well as in two-phase flow through porous media.

* Correspondence to: Department of Mechanical Engineering, National Technical University of Athens, PO Box 64070, 15710 Zografou, Athens, Greece.
[1] E-mail: sgt@fluid.mech.ntua.gr

Received November 1998
Revised June 1999

Copyright © 2000 John Wiley & Sons, Ltd.

There have been several theoretical and experimental studies of the motion of drops through two-dimensional channels and circular tubes. A recent numerical study is that of Martinez and Udell [3]. These authors obtained numerical solutions of the creeping flow equations using a boundary integral method (BIM). They performed a detailed examination of the effects of capillary number, viscosity ratio and drop size on the deformation and speed of the drop, as well as on the additional pressure loss due to the presence of the drop. Borhan and Mao [4] studied the effect of surfactants on the motion of drops through circular tubes using a BIM. Tsai and Miksis [5] studied the dynamics of a drop in a straight as well as constricted tube using a BIM. Manga [6] studied the dynamics of drops in branched two-dimensional channels using also a BIM. A recent experimental study is that of Olbricht and Kung [7]. They studied the deformation and break-up of liquid drops in low-Reynolds number flow through a capillary tube for sizes of drop comparable with the tube diameter. A recent review of research on drops may be found in Reference [8].

Here we study the motion of drops in two-dimensional channels and axisymmetric circular tubes, using a new method for this area of research. The method we use was introduced by Sussman *et al*. [9] for the two-dimensional case, and it was applied by them to study the motion of rising air bubbles in water and falling water drops in air for the case of ambient flow. This method uses a level set approach coupled with a projection methodology. With this approach, for each time step the velocity field is calculated initially by the solution of the two-dimensional, full Navier–Stokes equations for incompressible flow using a second-order projection method, which implements a second-order upwind procedure for differencing the convective terms. Then, using the computed velocity field, the interface is identified as the zero level set of a smooth function, which evolves in time by the velocity field. This approach allows for large density and viscosity ratios as well as surface tension. The important feature of the method is that the level set function is maintained as a distance function for all time without reconstructing the interface. This prevents the interface from ever changing thickness. The formulation automatically takes care of merging and breaking the interface.

We extend this method for the axisymmetric case and we apply it to a problem where the effect of bounding walls is evident. Results are compared for the two-dimensional case with results obtained by Audet [10] for solid cylindrical particles. In our problem, we simulate the solid particles as very viscous drops (viscosity ratio equal to 100). For the axisymmetric case, we compared our results with results obtained by Martinez and Udell [3]. For the two-dimensional case, we performed a study on the influence of the non-dimensional parameters of the problem on drop deformation, drop speed and on the additional pressure drop due to the presence of the drop. These results agree qualitatively with the results of Martinez and Udell [3] for the axisymmetric case.

The statement of the problem is presented in Figure 1. An initially cylindrical or spherical drop is placed in the inlet, at the centreline of a channel or tube respectively. The density of the drop is equal to the density of the suspending fluid, so there are no buoyancy effects. The viscosity of the drop is generally different from that of the suspending fluid. Surface tension forces may or may not act on the interface of two fluids. The undisturbed flow inside the tube can be developing Poiseuille or developed Poiseuille flow. The evolutions of shape of the drop as well as velocity and pressure fields are estimated as the drop travels along the channel or tube.

Copyright © 2000 John Wiley & Sons, Ltd.

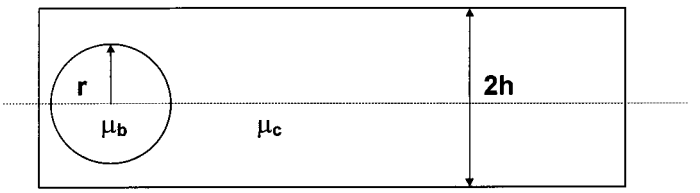

Figure 1. The initial ($t' = 0$) position and the shape of drop profile is shown. The initial velocity field is that of Poiseuille flow.

2. DESCRIPTION OF ALGORITHM

2.1. Equations of motion

In our study we shall consider the motion of cylindrical drops in two-dimensional channels and of spherical drops in circular straight tubes. We shall denote the viscosity inside the drop by μ_b and for the continuous phase by μ_c. The density of the drop is assumed equal to the density of the continuous phase and is denoted by ρ.

The equations of motion that govern the flow field are given by the incompressible Navier–Stokes equations excluding the body force and including a surface tension force

$$\mathbf{u}_t + (\mathbf{u}\cdot\nabla)\mathbf{u} = \frac{1}{\rho}\left(-\nabla p + \nabla\cdot(2\mu D) + \sigma\kappa\delta(d)\mathbf{n}\right) \tag{1}$$

$$\nabla\cdot\mathbf{u} = 0 \tag{2}$$

where $\mathbf{u} = (u, v)$ is the fluid velocity, ρ is the constant density for both fluids, $\mu = \mu(\mathbf{x}, t)$ is the function of fluid viscosity that is later determined by the constant viscosities of two fluids, and D is the rate of deformation tensor. The surface tension term is considered to be a force concentrated on the interface. We denote σ as the surface tension, κ as the curvature of the interface, d as the normal distance to the interface, δ as the Dirac delta function, and $\mathbf{n}$ as the unit outward normal vector at the interface.

2.2. Projection

The solution of the system of Equations (1) and (2) gives directly the velocity field of the flow. For the solution, a second-order projection method is used as follows:

From Equation (1) we have

$$L\mathbf{u} = \mathbf{u}_t + \nabla p/\rho \tag{3a}$$

$$L\mathbf{u} = \frac{1}{\rho}\left(\nabla\cdot(2\mu D) + \sigma\kappa\delta(d)\mathbf{n}\right) - (\mathbf{u}\cdot\nabla)\mathbf{u} \tag{3b}$$

Copyright © 2000 John Wiley & Sons, Ltd.

It is well established that if the initial value problem of Equations (3a) and (3b) is well posed, then there exists a unique decomposition (Hodge decomposition), whereby

$$L\mathbf{u} = \mathbf{V}_d + \nabla f \tag{4}$$

where $\mathbf{V}_d$ is divergence free, f is a scalar function and $\mathbf{V}_d \perp \nabla f$. Comparing Equations (3a) and (4) and taking into account that $\mathbf{u}_t$ is divergence free according to the continuity equation for incompressible fluids and p/ρ is a scalar function, it is concluded that Equation (3a) is the unique decomposition of $L\mathbf{u}$.

In order to compute $\mathbf{u}_t$ we take the curl of both sides of Equation (3a) to obtain

$$\nabla \times L\mathbf{u} = \nabla \times \mathbf{u}_t \tag{5}$$

as $\nabla \times \nabla p = 0$ by the definition of these operators. Given any divergence-free vector $\mathbf{V}_d$, there exists a vector potential Ψ, such that $\mathbf{V}_d = \nabla \times \Psi$. Therefore, we can write

$$\mathbf{u}_t = \nabla \times \Psi \tag{6}$$

Furthermore, in two dimensions or for axisymmetric fields, we have $\Psi = (0, 0, \psi)$. So, Equation (5) can now be written as

$$\nabla \times L\mathbf{u} = \nabla \times (\nabla \times \Psi) = \nabla(\nabla \cdot \Psi) - \nabla^2 \Psi \tag{7a}$$

Taking into account that $\Psi = (0, 0, \psi)$, we have $\nabla \cdot \Psi = 0$ and $\nabla^2 \Psi = \nabla^2 \psi$. Hence, Equation (7a) can be written as

$$-\nabla^2 \psi = \nabla \times L\mathbf{u} \tag{7b}$$

The right-hand side of Equation (7b) can be calculated by computing the curl of Equation (3b). So, if we define proper boundary conditions for ψ, we can estimate ψ from the solution of Equation (7b). We define boundary conditions for ψ, taking into account its definition as $\mathbf{u}_t = \nabla \times \Psi$, where $\Psi = (0, 0, \psi)$. From this definition it can be calculated that

$$u_t = \frac{\partial \psi}{\partial y} \quad \text{and} \quad v_t = -\frac{\partial \psi}{\partial x}$$

and

$$\mathrm{d}\psi = \left(\frac{\partial \psi}{\partial x}\right) \mathrm{d}x + \left(\frac{\partial \psi}{\partial y}\right) \mathrm{d}y = -v_t \, \mathrm{d}x + u_t \, \mathrm{d}y$$

For constant x we have $\mathrm{d}x = 0$ and the above equation becomes $\mathrm{d}\psi = u_t \, \mathrm{d}y$. Integrating this equation from the down wall to the upper wall of the channel (from 0 to $2h$) and taking into account the expression of the volume flow rate $Q = \int_0^{2h} u \, \mathrm{d}y$, we have the final equation

Copyright © 2000 John Wiley & Sons, Ltd.

$$\frac{dQ}{dt} = \psi_{2h} - \psi_0$$

where t denotes time. Hence, if we define the actual flow rate to the channel by imposing proper initial conditions for the velocity field, it must be for all t that $dQ/dt = 0$, so that $\psi_{2h} = \psi_0$ for $x =$ constant. In addition, at the walls or at the symmetry axis $v_t = -\partial\psi/\partial x = 0$, which means $\psi_{2h} = \psi_0 =$ constant for all the length of the pipe.

At the entrance and outlet of pipe we assume steady conditions, which means $u_t = \partial\psi/\partial y = 0$ and $v_t = -\partial\psi/\partial x = 0$. So, we can also define $\psi =$ constant at the entrance or the outlet of the pipe. As $\mathbf{u}_t = \nabla \times \Psi$, the time evolution of velocity field can be estimated from the solution of Equation (7b).

2.3. The level set formulation

In order to capture the interface, a level set technique is used. A level set function, ϕ, is defined at each point of the flow field as follows. At the point $P(x, y)$, the absolute value of ϕ is equal to the distance of this point from the drop interface. If the point $P(x, y)$ is inside the drop, ϕ is assigned a negative value, while if the point $P(x, y)$ is outside of drop, ϕ is assigned a positive value. The drop interface corresponds to points for which $\phi = 0$.

In order to compute the evolution of the drop interface in time, which means to compute how the points of flow field for which $\phi = 0$ move in time, we use the equation

$$\phi_t + (\mathbf{u}\cdot\nabla)\phi = 0 \tag{8}$$

This equation is equivalent with the equation $D\phi/Dt = 0$. $\phi = 0$ is the material curve of the drop interface and therefore it should move according to the equation $D\phi/Dt = 0$ from the definition of the material derivative D/Dt.

While ϕ is initially defined as a distance function from the drop interface, it will not remain so. Therefore, a way of reinitializing ϕ in order to remain a distance function is necessary. The method we used is described by Sussman *et al.* [9] and it is as follows. At each time instant, we estimate, by solving Equation (8), the function $\phi_0(\mathbf{x})$ whose zero level set is the interface of drop. $\phi_0(\mathbf{x})$ need not be a distance function, however. We construct a function $\phi(\mathbf{x})$ with the properties that its zero level set is the same as $\phi_0(\mathbf{x})$ and that $\phi(\mathbf{x})$ is the signed normal distance from the interface. This is achieved by solving the following problem to steady state:

$$\phi_t = S(\phi_0)(1 - \sqrt{\phi_x^2 + \phi_y^2}) \tag{9a}$$

$$\phi(\mathbf{x}, 0) = \phi_0(\mathbf{x}) \tag{9b}$$

where $S(\phi_0)$ is the sign function. For numerical purposes it is useful to smooth the sign function as

$$S(\phi_0) = \phi_0/\sqrt{\phi_0^2 + \varepsilon^2} \tag{10}$$

Copyright © 2000 John Wiley & Sons, Ltd.

Equations (9a) and (9b) have the property that ϕ remains unchanged at the interface. Therefore, the zero level set of ϕ and ϕ_0 are the same. Away from the interface, ϕ will converge to $|\nabla\phi| = \sqrt{\phi_x^2 + \phi_y^2} = 1$. Therefore, it will converge to the actual distance from the drop interface. The above algorithm completely avoids finding the interface and it proves to be efficient to implement numerically.

2.4. Smoothing

Special care must be taken when resolving the discontinuity of viscosity at the interface (at $\phi = 0$) and when computing the delta function that appears in the surface tension term. For these reasons, the interface is not kept completely sharp but it is given a finite thickness of the order of the mesh size to provide stability and smoothness. This thickness remains constant for all time but decreases with a finer resolution of the grid.

In order to determine the viscosity $\mu(\phi)$ at the interface, we use the following definition:

$$\mu(\phi) = \begin{cases} \mu_c & \text{if } \phi > a \\ \mu_b & \text{if } \phi < -a \\ \bar{\mu} - \Delta\mu \sin(\pi\phi/2a) & \text{otherwise} \end{cases} \tag{11}$$

where $2a$ is the thickness of the interface and the following definitions are used:

$$\bar{\mu} \equiv \frac{\mu_b + \mu_c}{2}$$

$$\Delta\mu = \frac{\mu_b - \mu_c}{2}$$

The surface tension force is represented in Equation (1) by $\mathbf{F} = \sigma\kappa\delta(d)\mathbf{n}\cdot\mathbf{F}$, and can be cast in the level set formulation and smoothed using

$$\mathbf{F} = \sigma\kappa\delta(d)\mathbf{n} = \sigma\kappa(\phi)\delta(\phi)\nabla\phi/|\nabla\phi| \tag{12}$$

where

$$\mathbf{n} = \nabla\phi/|\nabla\phi| \quad \text{and} \quad \kappa = \nabla\cdot\mathbf{n} = \nabla\cdot(\nabla\phi/|\nabla\phi|) \tag{13}$$

Because ϕ is maintained as a distance function we may numerically approximate $\delta(\phi)$ by a modified delta function, smoothed as follows:

$$\delta(\phi) = \begin{cases} (1/2)(1 + \cos(\pi\phi/a)/a) & \text{if } |\phi| < a \\ 0 & \text{otherwise} \end{cases} \tag{14}$$

where a is the prescribed half-thickness of the interface.

Copyright © 2000 John Wiley & Sons, Ltd.

The contribution of surface tension to the right-hand side of Equation (7b) is

$$\nabla \times \mathbf{F} = -\sigma((\kappa(\phi)\delta(\phi)\phi_y)_x - (\kappa(\phi)\delta(\phi)\phi_x)_y)) \tag{15}$$

If we write $\delta(\phi)$ as $\partial H(\phi)/\partial\phi$, we can reduce Equation (15) to

$$\nabla \times \mathbf{F} = -\sigma(\kappa(\phi)_x H_y - \kappa(\phi)_y H_x)) \tag{16}$$

The equation for H is

$$H(\phi) = \begin{cases} \dfrac{1}{2} & \text{if } \phi > a \\ -\dfrac{1}{2} & \text{if } \phi < -a \\ \dfrac{1}{2}\left(\dfrac{\phi}{a} + \dfrac{1}{\pi}\sin(\pi\phi/a)\right) & \text{otherwise} \end{cases} \tag{17}$$

Implicit in the above formulae is that ϕ is a distance function.

2.5. Pressure field estimation

Equation (3) can be written as

$$\nabla p = \rho(L\mathbf{u} - \mathbf{u}_t) \tag{18}$$

where $L\mathbf{u} = (V_1, V_2)$ and $\mathbf{u}_t = (u_t, v_t)$

V_1, V_2, u_t, v_t have been computed for the determination of the velocity field as it was described. Therefore, we have from Equation (18)

$$p_x = \rho(V_1 - u_t) \tag{19}$$

$$p_y = \rho(V_2 - v_t) \tag{20}$$

By integrating Equations (19) or (20), we can compute the pressure field. In order to compute the pressure field more accurately instead of using Equations (19) or (20), we construct and solve the following Equation (21). Adding Equations (19) and (20), we have the following equation for the pressure field:

$$p_x + p_y = \rho(V_1 + V_2) - \rho(u_t + v_t) \tag{21}$$

Copyright © 2000 John Wiley & Sons, Ltd.

In order to solve Equation (21) we use the following boundary conditions: at the upper wall, $p_y = 0$; at the axis of symmetry, $p_y = 0$; at the inlet, $p = 0$; and at the outlet, $p_x = C$, where C is a known quantity from Equation (19).

In the case that surface tension is active, Equation (21) does not work due to the discontinuity of p_x and p_y at the interface. In that case we solve Equation (19) at wall where surface tension is not active, so p is computed at the wall. Starting from each grid point of the wall, where p is known, and integrating Equation (20) perpendicular to the wall, i.e. along all y grid lines, p is computed at all grid points of flow field.

2.6. Discretization

The discretization of Equations (7b), (8) and (9) is described in detail by Sussman *et al*. [9] for the two-dimensional case. We have extended this discretization for the additional axisymmetric terms. Here, we briefly state the main features of discretization as it is described in the above-mentioned paper and we describe the discretization of Equations (19)–(21), which are used for the computation of pressure.

A staggered mesh is used for velocity and the level set function. With s as the mesh size, we define the points (i, j) at the centre of the cells and the points $(i-\frac{1}{2}, j-\frac{1}{2})$ at the corner of the cells

$$\mathbf{x}_{i,j} = ((i+\tfrac{1}{2})s, (j+\tfrac{1}{2})s)$$

$$\mathbf{x}_{i-1/2,j-1/2} = (is, js)$$

$$\mathbf{u}_{i,j} = \mathbf{u}(\mathbf{x}_{i,j})$$

$$\phi_{i,j} = \phi(\mathbf{x}_{i,j})$$

$$p_{i-1/2,j-1/2} = p(\mathbf{x}_{i-1/2,j-1/2})$$

$$\psi_{i-1/2,j-1/2} = \psi(\mathbf{x}_{i-1/2,j-1/2})$$

$$i = 0, \ldots, M-1, \qquad j = 0, \ldots, N-1$$

The discrete operators are defined for divergence, gradient and curl operators. The final difference formula of Equation (7b) that is used to estimate the function ψ is

$$\begin{aligned}&(1 - cs/y)\psi_{i-1/2,j-1/2} + (1 - cs/y)\psi_{i-1/2,j+3/2} + (1 + cs/y)\psi_{i+3/2,j-1/2}\\ &+ (1 + cs/y)\psi_{i+3/2,j+3/2} - 4\psi_{i+1/2,j+1/2} = -(\nabla \times L\mathbf{u})\end{aligned} \tag{22}$$

where $c = 0$ for the two-dimensional case and $c = 1$ for the axisymmetric case.

In the right-hand side of Equation (22), convection terms, viscous terms and the surface tension term are included. For the discretization of convection terms, a second-order essential non-oscillatory (ENO) method is used. For the discretization of viscous stress tensor, central

Copyright © 2000 John Wiley & Sons, Ltd.

differencing is applied. In order to compute the surface tension contribution, we compute the curvature $\kappa(\phi)$ of the interface and its derivatives (Equation (16)) with similar equations as those used for the computation of viscous terms. The system of algebraic equations (22) is solved by using a conjugate gradient method.

For evolution in time, a second-order Adams–Bashforth method is used. Similar equations are used for the time evolution of the level set equation (9). An upwind scheme, in that it differences in the direction of propagating characteristics, is used for the discretization of the transport equation (8) in order to avoid numerical instabilities, because at this transport equation there are no diffusion terms.

Equation (21), which is used for the computation of pressure when surface tension is not active, is discretized as follows:

$$(p_x)_{i,j} = (p_{i+1/2,j+1/2} - p_{i-1/2,j+1/2} + p_{i+1/2,j-1/2} - p_{i-1/2,j-1/2})/2s \tag{23a}$$

$$(p_y)_{i,j} = (p_{i+1/2,j+1/2} - p_{i+1/2,j-1/2} + p_{i-1/2,j+1/2} - p_{i-1/2,j-1/2})/2s \tag{23b}$$

Adding Equations (23a) and (23b) and taking into account Equation (21), we have

$$p_{i+1/2,j+1/2} - p_{i-1/2,j-1/2} = s(\rho(V_1 + V_2))_{i,j} - (\rho(u_t + v_t))_{i,j} \tag{24}$$

Equation (19), which is used when surface tension is active, is discretized as follows:

$$p_{i+1/2,N} - p_{i-1/2,N} = s(\rho(V_1 - u_t))_{i,N} \tag{25}$$

where N is the j grid line at the wall.

Equation (20) is integrated along j grid lines after estimation of pressure at the wall from Equation (25)

$$p_{i+1/2,j-1/2} = p_{i+1/2,j+1/2} - (p_y)_{i+1/2,j}\text{s}, \quad \text{for } j = N-1, 1 \tag{26}$$

This integration does not create problems as the drop interface is crossed, because when the interface is crossed, the actual value of p_y is used, which takes into account the surface tension and the change in viscosity at the interface. p_y is not continuous at the interface, but the summation of its actual value does not create problems, such that the solution of a differential equation including p_y would create.

Equations (24) and (25) are solved using a conjugate gradient method.

3. RESULTS AND DISCUSSION

In this section the results of the numerical computations are compared with existing results. In addition, results in terms of the effects of the non-dimensional parameters of the problems are presented and discussed.

Copyright © 2000 John Wiley & Sons, Ltd.

In both the two-dimensional and the axisymmetric cases, the non-dimensional parameters that appear and affect the solutions are

1. The relative size of drop to the size of the channel or tube, i.e. $k = r/h$ for the two-dimensional case and $k = r/R$ for the axisymmetric case, where r is the radius of the undeformed cylindrical or spherical drop at the inlet of the channel or tube respectively, h is the half-width of the channel and R is the radius of tube.
2. The ratio of drop viscosity μ_b to the suspending fluid viscosity μ_c, $\lambda = \mu_b/\mu_c$.
3. The capillary number $Ca = \mu_c V/\sigma$, where V is the mean velocity of flow and σ is the surface tension. Therefore, Ca is the ratio of viscous forces to surface tension forces.
4. The Reynolds number, i.e. $Re = \rho VD/\mu_c$, where D is the hydraulic diameter of the channel or tube.

As a non-dimensional variable, the non-dimensional time is used, $t' = tV/h$ for the two-dimensional problem and $t' = tV/R$ for the axisymmetric problem.

The values of parameters that were examined were chosen in such a way that a direct comparison with existing results, obtained by other methods, could be done and, in addition, the effect of variation of parameters for the two-dimensional case could be studied to some extent. Table I shows the values of parameters covered in the numerical computations. For each case we compute the evolution of drop shape as well as the additional pressure drop. The term additional pressure drop ΔP^+ is defined as the total pressure decrease over a distance extending into the undisturbed flow ahead of and behind the drop, less the Poiseuille value over the same distance and for the same volume flux of suspending fluid alone. The additional pressure drop represents the local pressure loss due solely to the presence of the drop.

3.1. Two-dimensional case

3.1.1. Comparison with existing results. In this section we compare our results with the results of Audet [10] for the motion of solid cylinders in channels. We model the solid cylinder as a very viscous drop (viscosity ratio $\lambda = 100$). The viscosity of the suspending fluid is taken equal to that used in the above-mentioned work. We study the motion of an initial cylindrical drop, with $k = 0.8$, $\lambda = 100$ and $Ca = \infty$.

In Figure 2, the evolution of the drop is presented, until its centre reaches the position $x/h = 4$. We see that it keeps almost its initial circular profile. Therefore, it could be a reasonable model for the solid cylinder.

In Figure 3, we compare the velocity profiles of flow at a distance $l = 1$ upstream of the centre of drop. We also found good agreement when comparing the speed of the drop:

Table I. Parameters covered in numerical computations.

	Two-dimensional case	Axisymmetric case
Drop size, k	0.4, 0.8	0.726, 0.9
Viscosity ratio, λ	0.2, 5, 100	10, 0.1
Capillary number, Ca	0.1, ∞	0.1, 1.0
Reynolds number, Re	$\ll 1$	$\ll 1$

Copyright © 2000 John Wiley & Sons, Ltd.

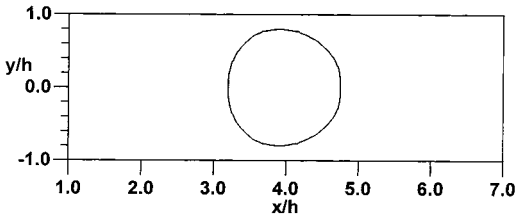

Figure 2. Evolution of an initially cylindrical drop with $k = 0.8$, $\lambda = 100$ and $Ca = \infty$ until its centre reaches position $x/h = 4$.

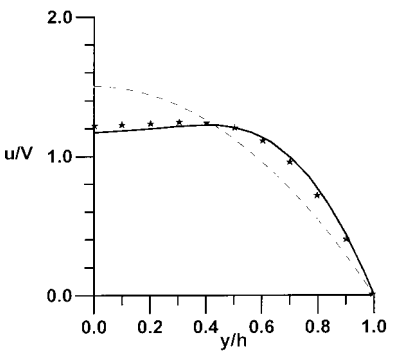

Figure 3. Velocity profile at position $l = 1$. Upstream of the centre of the drop, for $k = 0.8$, $\lambda = 100$ and $Ca = \infty$. —, Present results; ★★★, results from Audet [10]; – – –, Poiseuille flow without drop.

$U/V = 1.1$ in our results and $U/V = 1.13$ in the results of Audet [10], where U is the velocity of the drop and V is the mean velocity of the suspending fluid.

In Figure 4, we compare the pressure profile along the channel wall when the centre of the drop is at $x/h = 4$. We see from this figure that the additional pressure drop is greater in our results.

In Figure 5, we compare the pressure gradient along the channel wall when the centre of the drop is at $x/h = 4$.

In Figure 6, we compare the wall shear stress when the centre of the drop is at $x/h = 4$.

All the above comparisons agree qualitatively, but there are some quantitative differences, probably due to the fact that we used a finite viscosity ratio to model the solid cylinder.

3.1.2. Effect of drop size. The variations in drop shape with drop size are shown in Figure 7 for two values of k, $k = 0.4$ and 0.8. Both profiles are presented at time $t' = 3$. At time $t' = 0$, both drops were placed at the inlet of channel having a circular profile. Both shapes show a much higher curvature at the nose of the drop than at the trailing end. Actually, the curvature at the nose is positive while at the trailing end it is negative. The profile of a small drop is less deformed from the initial circular shape than the profile of a large drop, although the

Copyright © 2000 John Wiley & Sons, Ltd.

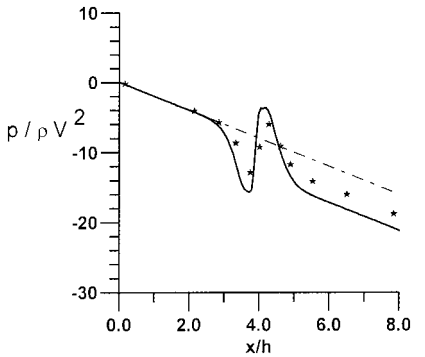

Figure 4. The pressure p along the channel wall. A drop of $k = 0.8$, $\lambda = 100$ and $Ca = \infty$ is on the channel centreline at $x/h = 4$. —, Present results; ★ ★ ★, results from Audet [10]; – – –, Poiseuille flow without drop.

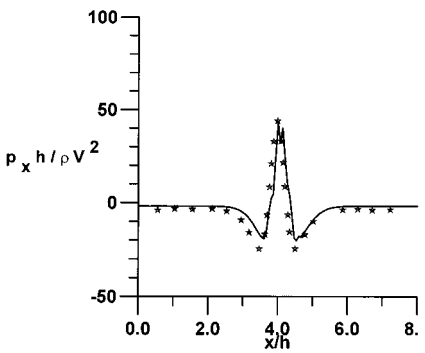

Figure 5. The pressure gradient p_x along the channel wall. A drop of $k = 0.8$, $\lambda = 100$ and $Ca = \infty$ is on the channel centreline at $x/h = 4$. —, Present results; ★ ★ ★, results from Audet [10].

deformation for both drops is large due to the lack of surface tension forces. For both drops, a steady shape does not exist, but the drops will continue to deform in their course through the channel, as computations have shown.

Estimating the velocity of a small drop from the distance that it travels in $t' = 3$, we see that it travels almost with a value of 1.5, which is the maximum velocity of flow for suspending fluid away from the drop at the centre of the channel. Thus, small drops move at nearly the local suspending fluid speed on the channel centreline, as it also reported by Martinez and Udell [3] for the axisymmetric case.

In Figure 8, the pressure at the wall is presented for both drops. We can see from this figure that for a small drop there is no remarkable additional pressure drop, while for a large drop there is.

Copyright © 2000 John Wiley & Sons, Ltd.

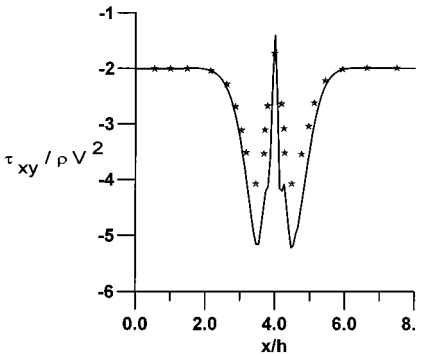

Figure 6. The wall shear stress τ_{xy}. A drop of $k = 0.8$, $\lambda = 100$ and $Ca = \infty$ is on the channel centreline at $x/h = 4$. —, Present results; ★ ★ ★, results from Audet [10].

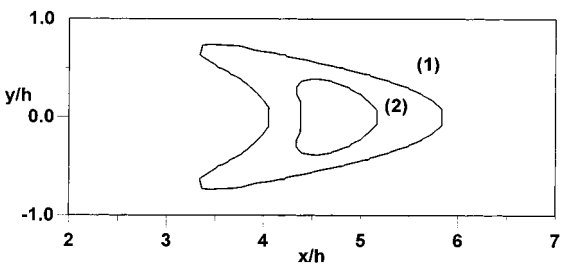

Figure 7. Effect of drop size k on drop shape at $t' = 3$ for $\lambda = 5$ and $Ca = \infty$. (1) $k = 0.8$, (2) $k = 0.4$.

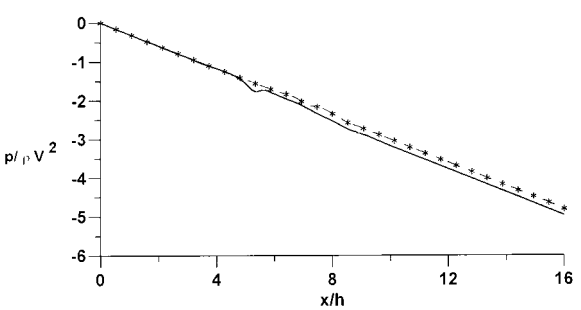

Figure 8. Effect of drop size k on pressure distribution across the channel at $t' = 3$ for $\lambda = 5$ and $Ca = \infty$. —, $k = 0.8$; ∗ ∗ ∗, $k = 0.4$; – – –, Poiseuille flow.

Copyright © 2000 John Wiley & Sons, Ltd.

3.1.3. Effect of viscosity ratio λ. In Figure 9, the velocity profiles at a position where the centre of the drop is located are presented for three different values of λ. The interface of the drop corresponds at the point of the curves where there is a discontinuity in the derivative of the velocity profile. We see that as λ increases, the shear rate inside the drop decreases and the profile of velocity becomes more blunt. We see also that velocity inside the drop decreases as λ increases, i.e. the drop speed decreases as λ increases. In addition, comparing curves (1), (2) and (3) with the Poiseuille profile, we see that for $\lambda > 1$, the velocity inside the drop is smaller than 1.5, i.e. the value predicted for Poiseuille flow of suspending fluid, while for $\lambda < 1$, the velocity inside the drop is greater than 1.5.

In Figure 10, the variations in drop shape with λ are shown for three different values of λ at $t' = 3$. For $\lambda = 100$, the profile of the drop does not deviate much from the initial circular profile. As λ decreases, the drop extends further in the axial direction and the jet of suspending

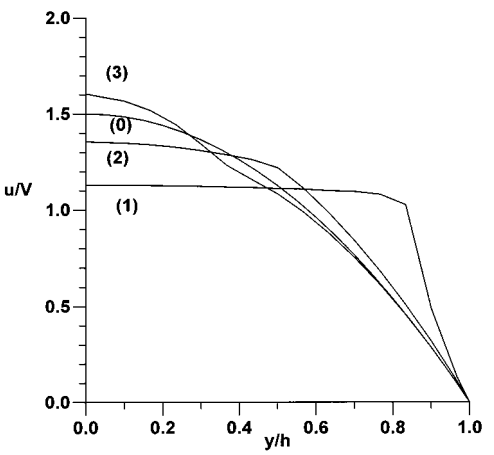

Figure 9. Effect of viscosity ratio λ on velocity profiles at the centre of the drops at $t' = 3$ for $k = 0.8$ and $Ca = \infty$. (1) $\lambda = 100$, (2) $\lambda = 5$, (3) $\lambda = 0.2$, (0) $\lambda = 1$ (Poiseuille flow).

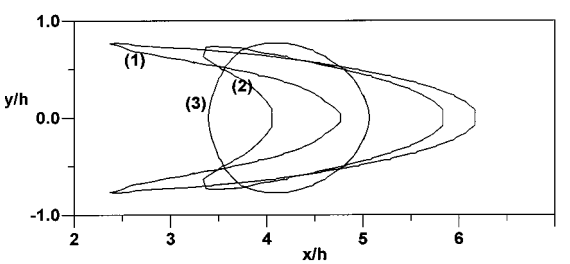

Figure 10. Effect of viscosity ratio λ on drop shape at $t' = 3$ for $k = 0.8$ and $Ca = \infty$. (1) $\lambda = 0.2$, (2) $\lambda = 5$, (3) $\lambda = 100$.

Copyright © 2000 John Wiley & Sons, Ltd.

fluid that penetrates into the trailing end of drop becomes larger. For $\lambda = 0.2$ and $\lambda = 5$, no steady shape of drop was obtained in the numerical computations.

In Figure 11, the pressure distribution at the wall of the channel is presented for the three different values of λ. We can see that ΔP^+ increases with λ as well as the variation of pressure at the wall over the drop. For the case of $\lambda = 0.2$, $\Delta P^+ < 0$, which means that the low viscosity drop can be transported with less pressure gradient than if the channel contained only suspending fluid flowing at the same bulk volume flux.

3.1.4. Effect of capillary number. In Figure 12, the variation in drop shape as affected by *Ca* is shown for two different values of *Ca*. From this figure we can see the strong effect of *Ca* on the drop deformation. For a large *Ca*, the deformation is large and the drop extends more in the direction of the flow. Moreover, the curvature at the leading end is larger for the large *Ca* and the curvature at the trailing end is negative, while for small *Ca* it is positive. In addition, for $Ca = 0.1$, a steady shape of drop exists, which is shown in the figure, while for $Ca = \infty$, a steady shape does not exist, i.e. drop deforms continuously.

In Figure 13, the pressure at the wall is presented for the above two values of *Ca*. From this figure we see that ΔP^+, as well as the variation in pressure at the wall over the drop is larger for the small value of *Ca*.

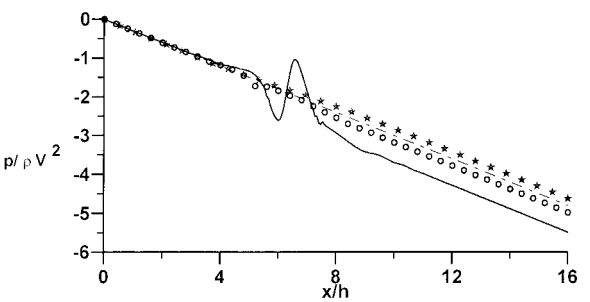

Figure 11. Effect of viscosity ratio λ on pressure distribution along the wall at $t' = 3$ for $k = 0.8$ and $Ca = \infty$. —, $\lambda = 100$; ○ ○ ○, $\lambda = 5$; ★ ★ ★, $\lambda = 0.2$; – – –, $\lambda = 1$ (Poiseuille flow).

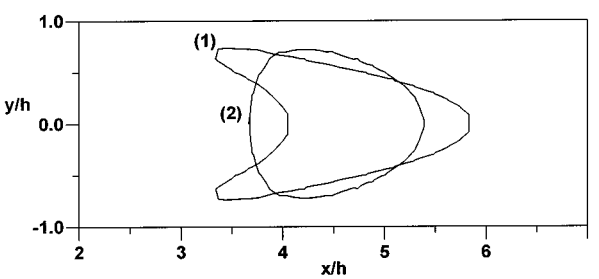

Figure 12. Effect of capillary number *Ca* on drop shape at $t' = 3$ for $k = 0.8$, $\lambda = 5$. (1) $Ca = \infty$, (2)

Copyright © 2000 John Wiley & Sons, Ltd.

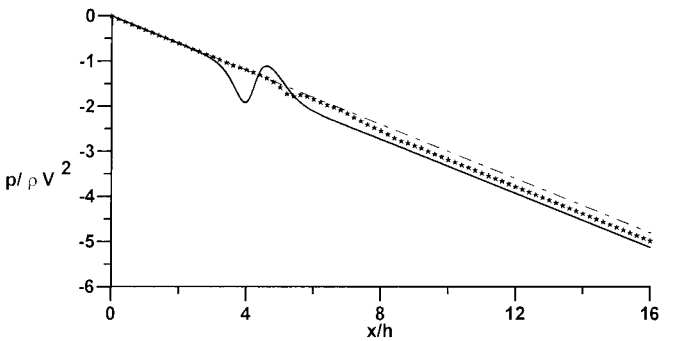

Figure 13. Effect of capillary number Ca on pressure distribution along the wall at $t' = 3$ for $k = 0.8$, $\lambda = 5$. ★★★, $Ca = \infty$; —, $Ca = 0.1$; – – –, Poiseuille flow.

3.2. Axisymmetric case

In Figure 14, the steady drop shape is compared with that presented by Martinez and Udell [3] for the same values of non-dimensional parameters.

In Figure 15, the pressure at the wall and the pressure at the centreline of the tube is presented. The dimensionless additional pressure drop $\Delta P^+ R/\mu V$ is 3.6. The value that Martinez and Udell [3] give for the same case is 3.4. From this figure we can see also the variation of pressure inside the drop. The pressure jump at the trailing end of the drop, as well as at the leading end, is due to surface tension forces that are localized at the interface of the drop.

In Figure 16, the general flow pattern of a drop that has reached in a permanent shape and translates with steady velocity in Poiseuille flow is illustrated. This figure shows the velocity vector field in and around a drop with the following non-dimensional parameters: $k = 0.73$, $\lambda = 10$, $Ca = 0.1$ for the axisymmetric case. The flow field is shown in a reference frame that moves at the drop velocity. In this frame a recirculation inside the drop appears. At the central portion of the drop there is a forward flow, while there is a backward flow close to the interface of the drop.

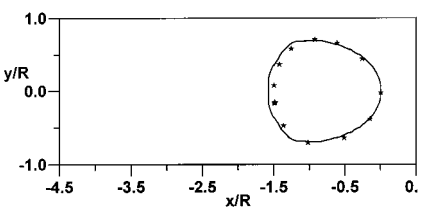

Figure 14. Comparison of steady drop shape with results of Martinez and Udell [3] for $k = 0.726$, $\lambda = 10$, $Ca = 0.1$. —, Present results; ★★★, results of Martinez and Udell [3].

Copyright © 2000 John Wiley & Sons, Ltd.

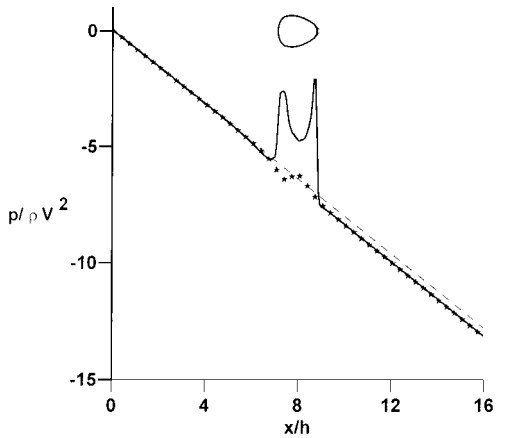

Figure 15. Pressure profile for a drop of $k = 0.726$, $\lambda = 10$, $Ca = 0.1$ at $t = 3$ s. ★★★, Along the tube wall; —, along the tube centreline; – – – Poiseuille profile.

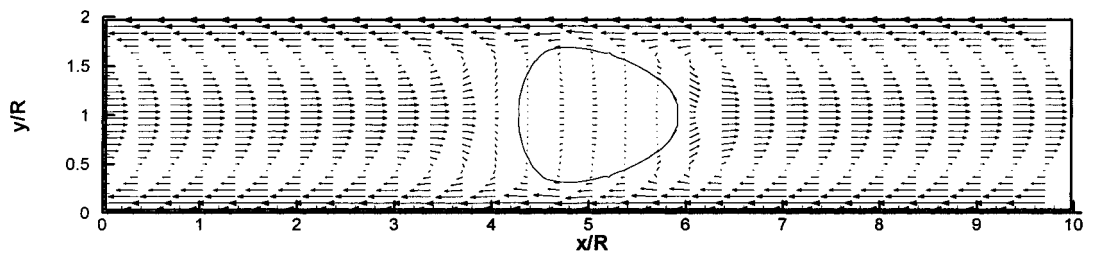

Figure 16. Velocity vector field for a drop of $k = 0.726$, $\lambda = 10$, $Ca = 0.1$ for the axisymmetric case, in a reference frame that moves with drop velocity.

At the interface of the drop the flow around the drop changes direction. This means the fluid close to the wall of the pipe moves with less velocity than the velocity of the drop, while the fluid close to the centreline of the pipe moves with a higher velocity than the velocity of the drop.

4. CONCLUSIONS

A level set approach coupled with a projection methodology was used to study the flow of a viscous drop in a channel and a tube filled with a second immiscible viscous fluid. The above technique was developed for the study of incompressible two-phase flow by Sussman *et al.* [9] for the two-dimensional case. The technique is extended for the axisymmetric case and we

Copyright © 2000 John Wiley & Sons, Ltd.

apply it, as far as we know, for first time to the case of motion of drops in channels and tubes, where there exists the influence of bounding walls. The present results are compared satisfactorily with results obtained by BIMs. In addition, numerical experiments are performed for the study of the two-dimensional case. The main conclusions from this study are: the results of the two-dimensional case agree qualitatively with those obtained by Martinez and Udell [3] for the axisymmetric case. For small capillary numbers or large viscosity ratios, there exist steady profiles that the viscous drops reach. For the other cases, drops deform continuously, elongate and a jet of suspending fluid enters the drop from the back. The shape of the drop depends strongly on capillary number. The additional pressure drop for less viscous drops than the suspending fluid may be negative for large capillary numbers. Generally, the additional pressure drop increases when capillary number decreases or viscosity ratio increases.

REFERENCES

1. Poulou S. A numerical model of the partitioning of particles at divergent bifurcations. PhD dissertation, Cornell University, 1995.
2. Queguiner C, Barthes-Biesel D. Axisymmetric motion of capsules through cylindrical channels. *Journal of Fluid Mechanics* 1997; **348**: 349–376.
3. Martinez MJ, Udell KS. Axisymmetric creeping motion of drops through circular tubes. *Journal of Fluid Mechanics* 1990; **210**: 565–591.
4. Borhan A, Mao CF. Effects of surfactants on the motion of drops through circular tubes. *Physics and Fluids A* 1992; **4**: 2628–2640.
5. Tsai TM, Miksis MJ. Dynamics of a drop in a constricted capillary tube. *Journal of Fluid Mechanics* 1994; **274**: 197–217.
6. Manga M. Dynamics of drops in branched tubes. *Journal of Fluid Mechanics* 1996; **315**: 105–117.
7. Olbricht WL, Kung DM. The deformation and break-up of liquid drops in low Reynolds number flow through a capillary. *Physics and Fluids A* 1992; **4**: 1347–1354.
8. Olbricht WL. Pore-scale prototypes of multiphase flow in porous media. *Annual Review in Fluid Mechanics* 1996; **28**: 187–213.
9. Sussman M, Smereka P, Osher S. A level set approach for computing solutions to incompressible two-phase flow. *Journal of Computational Physics* 1994; **114**: 146–159.
10. Audet DM. The numerical and experimental modelling of particle dynamics in branching tubes at low Reynolds numbers with an application to blood cell motion in capillary junctions. PhD dissertation, Cornell University, 1987.

Copyright © 2000 John Wiley & Sons, Ltd.